# A Quantitative Description of the Ground-State Wave Function of $Cu_A$ by X-ray Absorption Spectroscopy: Comparison to Plastocyanin and Relevance to Electron Transfer

**Serena DeBeer George,[†] Markus Metz,[†] Robert K. Szilagyi,[†] Hongxin Wang,[‡] Stephen P. Cramer,[‡] Yi Lu,[§] William B. Tolman,[⊥] Britt Hedman,*[,†,||] Keith O. Hodgson,*[,†,||] and Edward I. Solomon*[,†]**

*Contribution from the Department of Chemistry, Stanford University, Stanford, California 94305, Department of Applied Sciences, University of California, Davis, California, Physical Biosciences Division, Lawrence Berkeley National Laboratory, Berkeley, California 94720, Department of Chemistry, University of Illinois, Urbana, Illinois 61801, Department of Chemistry and Center for Metals in Biocatalysis, University of Minnesota, Minneapolis, Minnesota 55455, and Stanford Synchrotron Radiation Laboratory, SLAC, Stanford University, Stanford, California 94309*

*Received November 28, 2000. Revised Manuscript Received March 1, 2001*

**Abstract:** To evaluate the importance of the electronic structure of $Cu_A$ to its electron-transfer (ET) function, a quantitative description of the ground-state wave function of the mixed-valence (MV) binuclear $Cu_A$ center engineered into *Pseudomonas aeruginosa* azurin has been developed, using a combination of S K-edge and Cu L-edge X-ray absorption spectroscopies (XAS). Parallel descriptions have been developed for a binuclear thiolate-bridged MV reference model complex ($[(L^{iPrdacoS}Cu)_2]^+$) and a homovalent (II,II) analogue ($[L^{iPr2tacnS}Cu)_2]^{2+}$, where $L^{iPrdacoS}$ and $L^{iPr2tacnS}$ are macrocyclic ligands with attached thiolates that bridge the Cu ions. Previous studies have qualitatively defined the ground-state wave function of $Cu_A$ in terms of ligand field effects on the orbital orientation and the presence of a metal−metal bond. The studies presented here provide further evidence for a direct Cu−Cu interaction and, importantly, experimentally quantify the covalency of the ground-state wave function. The experimental results are further supported by DFT calculations. The nature of the ground-state wave function of $Cu_A$ is compared to that of the well-defined blue copper site in plastocyanin, and the importance of this wave function to the lower reorganization energy and ET function of $Cu_A$ is discussed. This wave function incorporates anisotropic covalency into the intra- and intermolecular ET pathways in cytochrome *c* oxidase. Thus, the high covalency of the Cys−Cu bond allows a path through this ligand to become competitive with a shorter His path in the intramolecular ET from $Cu_A$ to heme *a* and is particularly important for activating the intermolecular ET path from heme *c* to $Cu_A$.

## Introduction

There are two classes of copper-containing metalloproteins responsible for rapid intra- and intermolecular electron transfer in biological systems: those containing mononuclear blue copper sites[1−5] and those containing binuclear $Cu_A$ centers.[6−8] The blue copper (or type 1 Cu) center, found in plastocyanin, azurin, stellacyanin, and the multicopper oxidases, has a single Cu ion in a trigonally distorted tetrahedral environment (Figure 1a). The trigonal plane contains a single Cu ion with one S(Cys) and two N(His) ligands, where the Cu−S(Cys) bond is very short at ∼2.1 Å. In classic blue copper sites, such as azurin and plastocyanin, the axial ligand is a S(Met) having a long Cu−S bond length.[9] The $Cu_A$ center found in nitrous oxide reductase and cytochrome *c* oxidase is a completely delocalized (i.e., class III) mixed-valence binuclear center[10,11] in its oxidized state with two $Cu^{1.5+}$ separated by ∼2.4 Å and bridged by two S(Cys) (Figure 1b). The Cu centers are trigonal, with an N(His) providing the third equatorial ligand. The axial ligand on one Cu is an S(Met), and that on the second Cu is a polypeptide

* To whom correspondence should be addressed. Tel.: 650-723-9104. Fax: 650-725-0259. E-mail: edward.solomon@stanford.edu.
[†] Department of Chemistry, Stanford University.
[‡] University of California, Davis, and Lawrence Berkeley National Laboratory.
[§] University of Illinois.
[⊥] University of Minnesota.
[||] Stanford Synchrotron Radiation Laboratory.

(1) Adman, E. T. *Adv. Protein Chem.* **1991**, *42*, 145−198.
(2) Messerschmidt, A. *Struct. Bonding* **1998**, *90*, 37−68.
(3) Sykes, A. G. *Adv. Inorg. Chem.* **1991**, *107*, 377−408.
(4) Solomon, E. I.; Baldwin, M. J.; Lowery, M. D. *Chem. Rev.* **1992**, *92*, 521−542.
(5) Solomon, E. I.; Lowery, M. D. *Science* **1993**, *259*, 1575−1581.
(6) Beinert, H. *Eur. J. Biochem.* **1997**, *245*, 521−532.
(7) Ferguson-Miller, S.; Babcock, G. T. *Chem. Rev.* **1996**, *96*, 2889−2907.
(8) Ramirez, B. E.; Malmström, B. G.; Winkler, J. R.; Gray, H. B. *Proc. Natl. Acad. Sci. U.S.A.* **1995**, *92*, 11949−11951.
(9) In addition, several classes of perturbed blue copper sites exist, which include sites with a stronger field axial ligand (e.g., O(Gln) in stellacyanin: Hart, P. J.; Nersissian, A. M.; Herrmann, R. G.; Nalbandyan, R. M.; Valentine, J. S.; Eisenberg, D. *Protein Sci.* **1996**, *5*, 2175−2183), sites with no axial ligand (e.g., as in the fungal laccases: Xu, F.; Shin, W.; Brown, S. H.; Wahleithner, J.; Sundaram, U. M.; Solomon, E. I. *Biochim. Biophys. Acta* **1996**, *1292*, 303−311), and sites with the same ligand set which have undergone a tetragonal distortion relative to plastocyanin (e.g., nitrite reductase: Adman, E. T.; Godden, J. W.; Turley, S. *J. Biol. Chem.* **1995**, *270*, 27458−27474, and cucumber basic: Guss, J. M.; Merritt, E. A.; Phizackerley, R. P.; Freeman, H. C. *J. Mol. Biol.* **1996**, *259*, 686−705).
(10) Kroneck, P. M. H.; Antholine, W. E.; Riester, J.; Zumft, W. G. *FEBS Lett.* **1989**, *248*, 212−213.
(11) Kroneck, P. M. H.; Antholine, W. E.; Riester, J.; Zumft, W. G. *FEBS Lett.* **1988**, *242*, 70−74.

10.1021/ja004109i CCC: $20.00 
Published on Web 05/23/2001

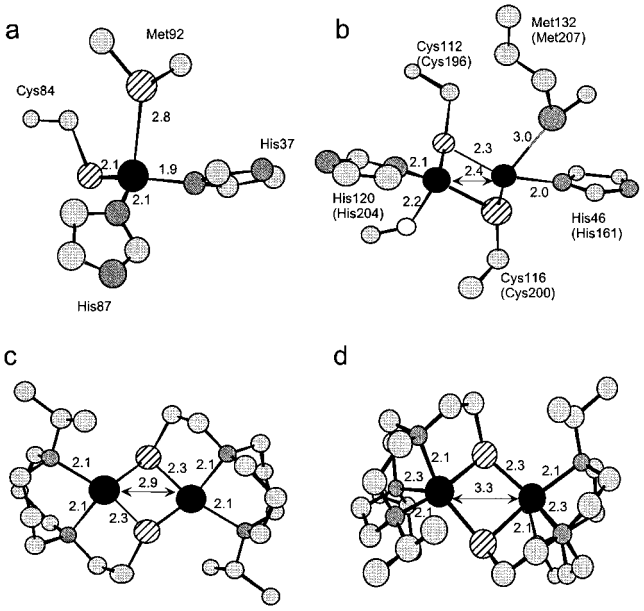


**Figure 1.** Structures of (a) plastocyanin (PDB 1PLC), (b) the engineered $Cu_A$ azurin construct (PDB 1CC3) (residue numbers given in parentheses are for bovine C*c*O), (c) the mixed-valence (MV) model complex, and (d) the homovalent (II,II) model. Distances are in angstrom units.

backbone carbonyl oxygen from Gln. Although geometrically quite different, blue copper and $Cu_A$ centers are both distinct from normal tetragonal copper sites in their spectral properties and their ability to perform rapid long-range electron transfer at rates on the order of $10^3-10^5$ $s^{-1}$.[12,13] The purpose of this study is to evaluate the electronic structure of $Cu_A$ relative to that of the well-understood blue copper site and to correlate differences in the electronic structures with their possible functional impact.

Over the past several decades, a vast amount of theoretical and experimental work has focused on correlating the electronic structure of blue copper centers with their electron-transfer (ET) function. Blue Cu centers generally show a very small parallel hyperfine splitting in the EPR spectrum and an intense S(Cys) $\pi \rightarrow$ Cu $d_{x^2-y^2}$ charge-transfer (CT) transition in the absorption spectrum, both reflecting the high anisotropic covalency of the Cu−thiolate bond.[12] This is directly observed in S K-edge X-ray absorption (XAS) spectra in which the intensity of the pre-edge feature at ~2740 eV provides electronic structural information about the singly occupied HOMO:[14]

$$\Psi_{HOMO} \approx [1 - \alpha^2]^{1/2} |\text{Cu } 3d\rangle - \alpha |\text{S } 3p\rangle - \beta |\text{other L}\rangle$$

Specifically, the intensity of the S K-pre-edge feature (i.e., S 1s → HOMO, where the S 1s → S 3p transition is electric dipole-allowed) provides an experimental measure of the thiolate covalency. This covalency is defined by $\alpha^2$, the sulfur 3p character contained in the metal d-derived molecular orbital. In this expression for $\Psi_{HOMO}$, $\beta^2$ corresponds to the other (non-sulfur) ligand character in the ground state. For the blue Cu center in plastocyanin, this method quantifies the S(Cys) character in the $Cu^{2+}$ $d_{x^2-y^2}$ orbital as 38%.[14] In an analogous manner, the dipole-allowed Cu 2p → 3d transition observed at the Cu L-edge quantifies the Cu 3d character in the half-occupied HOMO of plastocyanin, giving a complementary value of 41% Cu d (i.e., $(1 - \alpha^2 - \beta^2)$).[15] Together, these two experimental techniques provide direct experimental evidence of the highly anisotropic Cu−thiolate bond and give a quantitative description of the ground-state wave function in plastocyanin. This description is of particular importance to the ET function of blue copper sites, where the highly anisotropic covalency is important for coupling into ET pathways.[16] A recent pathways analysis of the multicopper oxidase ceruloplasmin provides an illustrative example.[17]

Although recent reports of several protein crystal structures containing $Cu_A$ centers[18−24] have spurred detailed studies on the $Cu_A$ site,[25−27] the electronic description of $Cu_A$ and its contribution to the function is not yet developed to the level of plastocyanin. Previously, calculations were applied to simplified model systems to obtain qualitative insight into the electronic structure and ground-state spectroscopic data.[25,27] The $Cu_A$ center is a mixed-valence binuclear center, and studies have focused on defining contributions to this delocalization and its contribution to the redox properties of the site.[25,26] This delocalization derives from the interaction between the two Cu ions ($2H_{Cu-Cu}$), which can be quantified from the $\psi \rightarrow \psi^*$ transition energy, where $\psi$ and $\psi^*$ are the bonding (occupied) and antibonding (singly occupied HOMO) molecular orbitals distributed over the two Cu centers. Both the bridging ligands (indirect superexchange pathways) and direct metal orbital overlap (a metal−metal bond) contribute to electron delocalization in $Cu_A$.

An important part of understanding the spectroscopy of $Cu_A$ has been achieved through parallel studies on a mixed-valence (MV) model complex,[28] shown in Figure 1c (and a homovalent analogue,[29] Figure 1d). This MV model (Figure 1c) has two thiolate bridges and complete electron delocalization, but the

(12) Solomon, E. I.; Penfield, K. W.; Gewirth, A. A.; Lowery, M. D.; Shadle, S. E.; Guckert, J. A.; LaCroix, L. B. *Inorg. Chim. Acta* **1996**, *243*, 67−78.

(13) Winkler, J. R.; Malmström, B. G.; Gray, H. B. *Biophys. Chem.* **1995**, *54*, 199−209.

(14) Shadle, S. E.; Penner-Hahn, J. E.; Schugar, H. J.; Hedman, B.; Hodgson, K. O.; Solomon, E. I. *J. Am. Chem. Soc.* **1993**, *115*, 767−776.

(15) George, S. J.; Lowery, M. D.; Solomon, E. I.; Cramer, S. P. *J. Am. Chem. Soc.* **1993**, *115*, 2968−2969.

(16) Lowery, M. D.; Guckert, J. A.; Gebhard, M. S.; Solomon, E. I. *J. Am. Chem. Soc.* **1993**, *115*, 3012−3013.

(17) Machonkin, T. E.; Solomon, E. I. *J. Am. Chem. Soc.* **2000,** *122*, 12547−12560.

(18) Iwata, S.; Ostermeier, C.; Ludwig, B.; Michel, H. *Nature* **1995**, *376*, 660−669.

(19) Ostermeier, C.; Harrenga, A.; Ermler, U.; Michel, H. *Proc. Natl. Acad. Sci. U.S.A.* **1997**, *94*, 10547−10553.

(20) Tsukihara, T.; Aoyama, H.; Yamashita, E.; Tomizaki, T.; Yamaguchi, H.; Shinzawa-Itoh, K.; Nakashima, R.; Yaono, R.; Yoshikawa, S. *Science* **1995**, *269*, 1069−1074.

(21) Tsukihara, T.; Aoyama, H.; Yamashita, E.; Tomizaki, T.; Yamaguchi, H.; Shinzawa-Itoh, K.; Nakashima, R.; Yaono, R.; Yoshikawa, S. *Science* **1996**, *272*, 1136−1144.

(22) Williams, P. A.; Blackburn, N. J.; Sanders, D.; Bellamy, H.; Stura, E. A.; Fee, J. A.; McRee, D. E. *Nat. Struct. Biol.* **1999**, *6*, 509−516.

(23) Robinson, H.; Ang, M. C.; Gao, Y.-G.; Hay, M. T.; Lu, Y.; Wang, A. H.-J. *Biochemistry* **1999**, *38*, 5676−5683.

(24) Brown, K.; Tegoni, M.; Prudêncio, M.; Pereira, A. S.; Besson, S.; Moura, J. J.; Moura, I.; Cambillau, C. *Nat. Struct. Biol.* **2000**, *7*, 191−195.

(25) Gamelin, D. R.; Randall, D. W.; Hay, M. T.; Houser, R. P.; Mulder, T. C.; Canters, G. W.; de Vries, S.; Tolman, W. B.; Lu, Y.; Solomon, E. I. *J. Am. Chem. Soc.* **1998**, *120*, 5246−5263.

(26) Williams, K. R.; Gamelin, D. R.; LaCroix, L. B.; Houser, R. P.; Tolman, W. B.; Mulder, T. C.; de Vries, S.; Hedman, B.; Hodgson, K. O.; Solomon, E. I. *J. Am. Chem. Soc.* **1997**, *119*, 613−614. Note that the previous S K-edge data on $Cu_A$ and the MV model underestimated the S covalency due to partial reduction of the samples.

(27) Neese, F.; Kappl, R.; Zumft, W. G.; Hüttermann, J.; Kroneck, P. M. H. *J. Biol. Inorg. Chem.* **1998**, *3*, 53−67. See also earlier references: Neese, F.; Zumft, W. G.; Antholine, W. E.; Kroneck, P. M. H. *J. Am. Chem. Soc.* **1996**, *118*, 8692−8699. Farrar, J. A.; Neese, F.; Lappalainen, P.; Kroneck, P. M. H.; Saraste, M.; Zumft, W. G.; Thomson, A. J. *J. Am. Chem. Soc.* **1996**, *118*, 11501−11514.

(28) Houser, R. P.; Young, V. G., Jr.; Tolman, W. B. *J. Am. Chem. Soc.* **1996**, *118*, 2101−2102.

2.9 Å Cu−Cu distance precludes direct metal−metal bonding. Using the MV model complex as a reference, it was found that Cu−Cu bonding contributes ∼7800 $cm^{-1}$ to the electronic coupling interaction between the Cu ions.[25,26] This intermetal bonding, combined with the strong Cu−S interaction (vide infra), gives a relatively large interaction ($H_{Cu-Cu}$), which keeps the $Cu_A$ site delocalized in the low-symmetry protein environment. This delocalization is considered to be an important factor in lowering both the inner- and outer-sphere reorganization energies in ET reactions.

Our previous studies on $Cu_A$ provided a qualitative description of its ground-state wave function in terms of ligand field effects on orbital orientation and the presence of a metal−metal bond.[25] In this study, we expand our preliminary S K-edge studies[26] on $Cu_A$, the mixed-valence reference model, and the homovalent (II,II) analogue and extend these studies to the Cu L-edge in order to obtain a quantitative description of the ground-state wave function of $Cu_A$. Specifically, this study focuses on the $Cu_A$ center of an engineered $Cu_A$ azurin construct,[30] which has been shown through detailed spectroscopic studies[25,26,30−34] and X-ray crystallography[23] to be an excellent reproduction of the $Cu_A$ site in cytochrome *c* oxidase and nitrous oxide reductase. Analysis of the S K-edge and Cu L-edge energies and transition intensities relative to the MV model, in conjunction with DFT calculations, provide further evidence for a metal−metal bonding interaction and quantitatively define the ground-state wave function of $Cu_A$. This wave function is compared to that of the well-defined blue copper site in plastocyanin, and the importance of the wave function to reduced reorganization energy and ET function in these sites are discussed. Finally, this wave function is used evaluate the contribution of anisotropic covalency to possible intra- and intermolecular ET pathways in cytochrome *c* oxidase.

## Experimental Section

**A. Sample Preparation.** The $Cu_A$ construct engineered into *Pseudomonas aeruginosa* azurin[30] and the synthetic mixed-valence ($[(L^{iPrdacoS}Cu)_2]^+$)[28] and homovalent ($[L^{iPr2tacnS}Cu)_2]^{2+}$)[29] models were prepared as described previously.

**B. X-ray Absorption Spectroscopy and Measurements and Data Analysis.** All data were measured at the Stanford Synchrotron Radiation Laboratory under ring conditions of 3.0 GeV and 60−100 mA.

**(i) S K-Edges.** S K-edge data were measured using the 54-pole wiggler beam line 6-2 in high magnetic field mode of 10 kG with a Ni-coated harmonic rejection mirror and a fully tuned Si(111) double-crystal monochromator. Details of the optimization of this setup for low-energy studies have been described in an earlier publication.[35] S K-edge measurements were made at room temperature for the solid samples and at ∼4 °C for the proteins. Solid samples were ground into a fine powder and dispersed as thinly as possible on Mylar tape to minimize the possibility of fluorescence saturation effects as described in ref 36. Protein samples were pre-equilibrated in a water-saturated He atmosphere for ∼0.5−1 h to minimize bubble formation in the sample cell. Protein solutions were loaded via syringe into a Pt-coated Al block sample holder with a 6.35-$\mu$m-thick polypropylene window. For the $Cu_A$ azurin construct samples, the protein concentration was 2.0 mM in 50 mM acetate buffer. The data were measured as fluorescence excitation spectra utilizing an ionization chamber as a fluorescence detector.[37,38] To check for reproducibility, two or three scans were measured for each of the solid samples. Two separate preparations of the $Cu_A$ azurin construct were run, and in both cases multiple scans were used to monitor for potential effects of photoreduction. The protein samples showed no signs of photoreduction during the first two scans; however, a small amount of photoreduction (<3%) could be seen by the third scan. The samples were reoxidized using 1 equiv of a 100 mM solution of $K_3[Fe(CN)_6]$ in 50 mM acetate buffer. After reoxidation, the samples again showed signs of photoreduction during the third scan. The data represent a four-scan average for the $Cu_A$ azurin construct, which includes two scans before reoxidation and two scans after reoxidation (i.e., only those scans which showed no signs of photoreduction were included in the averaged data). The energy was calibrated from S K-edge spectra of $Na_2S_2O_3 \cdot 5H_2O$, run at intervals between sample scans. The maximum of the first pre-edge feature in the spectrum was fixed at 2472.02 eV. A step size of 0.08 eV was used over the edge region. Data were averaged, and a smooth background was removed from all spectra by fitting a polynomial to the pre-edge region and subtracting this polynomial from the entire spectrum. Normalization of the data was accomplished by fitting a flattened polynomial or straight line to the post-edge region and normalizing the edge jump to 1.0 at 2490 eV. Fits to the edges were performed using the program EDG_FIT.[39] Second-derivative spectra were used as guides to determine the number and position of peaks. Pre-edge and rising edge features were modeled by pseudo-Voigt line shapes. For the pre-edge feature, a fixed 1:1 ratio of Lorentzian to Gaussian contributions was used. Fits were performed over several energy ranges. The reported intensity values and standard deviations are based on the average of all good fits. Normalization procedures can introduce ∼3% error in the total pre-edge peak areas, in addition to the error resulting from the fitting procedure.

**(ii) Cu L-Edges.** Cu L-edge data were measured using the 31-pole wiggler beam line 10-1 and bending magnet beam line 8-2. Cu L-edge measurements were made at room temperature for the solid samples and at ∼10 K for the proteins. Solid samples were finely ground and spread across double-adhesive conductive carbon tape, which was attached to an aluminum paddle. The $Cu_A$ azurin construct was run as a partially dehydrated film, prepared by placing ∼20 $\mu$L of 0.5 mM protein in 50 mM acetate buffer on a silicon plate at 4 °C and evaporating under partial vacuum. Total electron yield from the solid samples was measured using a Galileo 4716 channeltron electron multiplier as a detector. Fluorescent X-rays from the protein samples were detected using a windowless 13-element germanium array detector (Canberra Industries, GUL00505). For each solid sample, three or four scans were measured in order to check reproducibility, while for proteins, multiple scans were measured to monitor for photoreduction. All data represent single scans. The energy was calibrated from the Cu L-edge spectra of $CuF_2$, run at intervals between sample scans. The maxima of the $L_3$ and $L_2$ pre-edges were fixed at 930.5 and 950.5 eV, respectively. A step size of 0.1 eV was used over the edge region. A linear background was fit to the $L_3$-pre-edge region (870−920 eV) and was subtracted from the entire spectrum. Normalization was accomplished by fitting a straight line to the post-edge region and normalizing the edge jump to 1.0 at 1000 eV. Fits to the edges were performed using EDG_FIT.[39] A pseudo-Voigt peak was used to model the $L_3$ and $L_2$ $2p \rightarrow 3d$ transitions. Arctangent functions were used to model the $L_3$- and $L_2$-edge jumps. The total L-pre-edge intensity

(29) Houser, R. P.; Halfen, J. A.; Young, V. G., Jr.; Blackburn, N. J.; Tolman, W. B. *J. Am. Chem. Soc.* **1995**, *117*, 10745−10746.
(30) Hay, M.; Richards, J.; Lu, Y. *Proc. Natl. Acad. Sci. U.S.A.* **1996**, *93*, 461−464.
(31) Andrew, C. R.; Lappalainen, P.; Saraste, M.; Hay, M. T.; Lu, Y.; Dennison, C.; Canters, G. W.; Fee, J. A.; Slutter, C. E.; Nakamura, N.; Sanders-Loehr, J. *J. Am. Chem. Soc.* **1995**, *117*, 10759−10760.
(32) Blackburn, N. J.; Ralle, M.; Sanders, D.; Fee, J. A.; de Vries, S.; Houser, R. P.; Tolman, W. B.; Hay, M. T.; Lu, Y. *ACS Symp. Ser.* **1998**, *692*, 241−259.
(33) Hay, M. T.; Ang, M. C.; Gamelin, D. R.; Solomon, E. I.; Antholine, W. E.; Ralle, M.; Blackburn, N. J.; Massey, P. D.; Wang, X. T.; Kwon, A. H.; Lu, Y. *Inorg. Chem.* **1998**, *37*, 191−198.
(34) Wang, X.; Ang, M. C.; Lu, Y. *J. Am. Chem. Soc.* **1999**, *121*, 2947−2948.
(35) Hedman, B.; Frank, P.; Gheller, S. F.; Roe, A. L.; Newton, W. E.; Hodgson, K. O. *J. Am. Chem. Soc.* **1988**, *110*, 3798−3805.
(36) Shadle, S. E.; Hedman, B.; Hodgson, K. O.; Solomon E. I. *J. Am. Chem. Soc.* **1995**, *117*, 2259−2272
(37) Stern, E. A.; Heald, S. M. *Rev. Sci. Instrum.* **1979**, *50*, 1579−1582.
(38) Lytle, F. W.; Greegor, R. B.; Sandstrom, D. R.; Marques, E. C.; Wong, J.; Spiro, C. L.; Huffman, G. P.; Huggins, F. E. *Nucl. Instrum. Methods* **1984**, *226*, 542−548.
(39) George, G. N. *EDG_FIT*; Stanford Synchrotron Radiation Laboratory, Stanford Linear Accelerator Center, Stanford University, Stanford, CA 94309

reported here was calculated as $L_3 + L_2$. The reported intensity values and standard deviations are based on the average of all good fits. Normalization procedures can introduce ~4% error in total pre-edge peak area, in addition to the error resulting from the fitting procedure.

**C. Electronic Structure Calculations.** Hybrid density functional calculations were carried out using Gaussian98[40] on a Silicon Graphics Origin 2000 multiprocessor computer. The Becke three-parameter exchange and Lee−Yang−Parr correlation functionals were used as implemented in the software package (B3LYP[41−43]). The double-$\zeta$ quality, Ahlrichs-type all-electron basis set was employed for the Cu atom (62111111/33111/311) with additional (p,d,f) polarization functions.[44] The standard 6-31G(d) basis set was selected for all other atoms.[45−47] This combination of basis sets (480 Gaussians with 976 primitives) has been previously shown to be reasonable for a range of Cu-containing systems.[48,49] Several other basis sets and various other density functionals were tested,[50] and this level of theory was confirmed to have converged (i.e., improving the basis set and/or changing the level of theory did not significantly change the ground-state wave function).

The active site model was constructed from imidazole, methyl thiolate, dimethyl thioether, and *N*-methylethylamide fragments (Chart 1). The atomic coordinates (Supporting Information) were taken from the 1.65 Å resolution X-ray structure of the engineered $Cu_A$ azurin construct.[23] No symmetry constraints were applied in the calculations.

Population analysis of the ground-state wave function was carried out using Mulliken and Weinhold population analyses methods as they are implemented in the Gaussian98 software package.[51−54] The density functional wave functions (i.e., the Kohn−Sham orbitals) were calculated in two ways. First, a spin-restricted calculation (ROB3LYP, $\langle S^2 \rangle = 0.75$) was carried out as the simplest description of an open-shell system. In this case, the total spin density is reflected in either the αHOMO or the $\beta$LUMO wave functions (referred to above as the singly occupied HOMO), since all other orbitals are either doubly occupied or doubly unoccupied. However, since the spin polarization is important, spin-unrestricted calculations (UB3LYP, $\langle S^2 \rangle \approx 0.75$) were also performed. One of the major differences between the two treatments is that, in the latter case, the αHOMO does not necessarily reflect the total spin density, whereas the $\beta$LUMO does reflect the excess α-electron density.

**Chart 1**

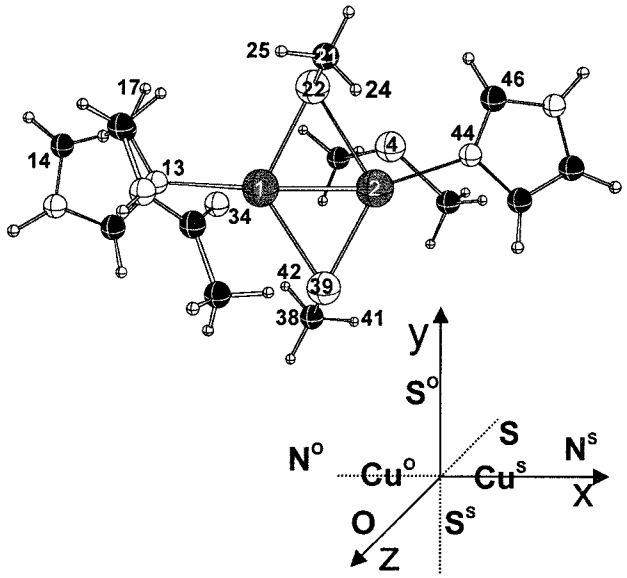


Since the XAS technique involves transitions to electron holes of the ground-state wave function, quantitation of the $\beta$LUMO is essential. In the spin-restricted case, the αHOMO equals the $\beta$LUMO; therefore, the calculated spin densities correspond directly to the electron hole wave function. In the spin-unrestricted treatment, a simple modification of the conventional population analysis was employed. The spin-up (α) and spin-down ($\beta$) Kohn−Sham orbitals ($\Psi_{ref}$) were interchanged ($\Psi_{inter}$) and used in the population analysis without further orbital coefficient optimization. The orbital occupations were kept as they were in the reference wave function. This transformation gives a "singly occupied $\beta$LUMO" and an "unoccupied αHOMO", while the doubly occupied spin-up ($\{\alpha\}$) and spin-down ($\{\beta\}$) orbitals do not change. To quantify the spin density due to spin polarization of the doubly occupied orbitals, $\Psi_{ox}$ was introduced, in which the αHOMO of $\Psi_{ref}$ is unoccupied. The pure $\beta$LUMO population was obtained according to the formula:

$$\begin{aligned} \mathrm{Pop}(\beta\mathrm{LUMO}) &= \mathrm{Spin}(\Psi_{inter}) + \mathrm{Spin}(\Psi_{ox}) \\ &= [\,\mathrm{Pop}(\beta\mathrm{LUMO} + \{\beta\}) - \mathrm{Pop}(\{\alpha\})\,] + \\ &\qquad [\,\mathrm{Pop}(\{\alpha\}) - \mathrm{Pop}(\{\beta\})\,] \quad (1) \end{aligned}$$

where Spin and Pop are obtained from a Mulliken or Weinhold population analysis, $\Psi_{ref} = (\alpha\mathrm{HOMO} + \{\alpha\},\{\beta\})$, $\Psi_{inter} = (\beta\mathrm{LUMO} + \{\beta\},\{\alpha\})$, and $\Psi_{ox} = (\{\alpha\}, \{\beta\}) = -(\{\beta\},\{\alpha\})$.

## Results and Analysis

**A. S K-Edges. (i) Pre-edge Intensities.** A comparison of the normalized S K-edge spectra for the $Cu_A$ azurin construct, the MV model, the homovalent (II,II) model, and plastocyanin[14] is shown in Figure 2a. The renormalized spectra (Figure 2b) account for the fact that a different number of sulfur atoms contribute to the pre-edge and edge features.[55] All four samples exhibit a pre-edge maximum between 2469 and 2471 eV. The renormalized spectra show similar pre-edge intensities for the $Cu_A$ azurin construct, the MV model, and homovalent model, while the intensity of plastocyanin is greater (Table 1).

The similar pre-edge intensities for $Cu_A$ and the two model complexes imply that the sulfur covalencies of these complexes are very similar (without renormalizing for the number of

(40) Frisch, M. J.; Trucks, G. W.; Schlegel, H. B.; Scuseria, G. E.; Robb, M. A.; Cheeseman, J. R.; Zakrzewski, V. G.; Montgomery, J. A. J.; Stratmann, R. E.; Burant, J. C.; Dapprich, S.; Millam, J. M.; Daniels, A. D.; Kudin, K. N.; Strain, M. C.; Farkas, O.; Tomasi, J.; Barone, V.; Cossi, M.; Cammi, R.; Mennucci, B.; Pomelli, C.; Adamo, C.; Clifford, S.; Ochterski, J.; Petersson, G. A.; Ayala, P. Y.; Cui, Q.; Morokuma, K.; Malick, D. K.; Rabuck, A. D.; Raghavachari, K.; Foresman, J. B.; Cioslowski, J.; Ortiz, J. V.; Stefanov, B. B.; Liu, G.; Liashenko, A.; Piskorz, P.; Komaromi, I.; Gomperts, R.; Martin, R. L.; Fox, D. J.; Keith, T.; Al-Laham, M. A.; Peng, C. Y.; Nanayakkara, A.; Gonzalez, C.; Challacombe, M.; Gill, P. M. W.; Johnson, B.; Chen, W.; Wong, M. W.; Andres, J. L.; Head-Gordon, M.; Replogle, E. S.; Pople, J. A. *Gaussian 98*, Revision A.1; Gaussian, Inc.: Pittsburgh, PA, 1998.

(41) Becke, A. D. *Phys. Rev. A* **1988**, *38*, 3098−3100.

(42) Lee, C.; Yang, W.; Parr, R. G. *Phys. Rev. B* **1988**, *37*, 785−789.

(43) Becke, A. D. *J. Chem. Phys.* **1993**, *98*, 5648−5652.

(44) Schafer, A.; Horn, H.; Ahlrichs, R. *J. Chem. Phys.* **1992**, *97*, 2571−2577.

(45) Hariharan, P. C.; Pople, J. A. *Theor. Chim. Acta* **1973**, *28*, 213−222.

(46) Francl, M. M.; Petro, W. J.; Hehre, W. J.; Binkley, J. S.; Gordon, M. S.; DeFree, D. J.; Pople, J. A. *J. Chem. Phys.* **1982**, *77*, 3654−3665.

(47) Rassolov, V.; Pople, J. A.; Ratner, M.; Windus, T. L. *J. Chem. Phys.* **1998**, *109*, 1223−1229.

(48) Ryde, U.; Olsson, M. H. M.; Pierloot, K. In *Theoretical Biochemistry; Process and Properties of Biological Systems*; Eriksson, L., Ed.; Elsevier: Amsterdam, 2001.

(49) Siegbahn, P. E. M.; Blomberg, M. R. A. *Chem. Rev.* **2000**, *100*, 421−437.

(50) Szilagyi, R. K.; Metz, M.; Solomon, E. I., unpublished results.

(51) Foster, J. P.; Weinhold, F. *J. Am. Chem. Soc.* **1980**, *102*, 7211−7218.

(52) Carpenter, J. E.; Weinhold, F. *J. Mol. Struct. (THEOCHEM)* **1988**, *169*, 41−62.

(53) Reed, A. E.; Curtis, L. A.; Weinhold, F. *Chem. Rev.* **1988**, *88*, 899−926.

(54) There are known limitations in population analyses with regard to atomic point charges; therefore, these are not discussed in the text. However, from tests on different Cu systems, the total atomic and gross orbital spin densities can give chemical insight into the ground-state wave function and show very similar results, regardless of the population analyses method employed.

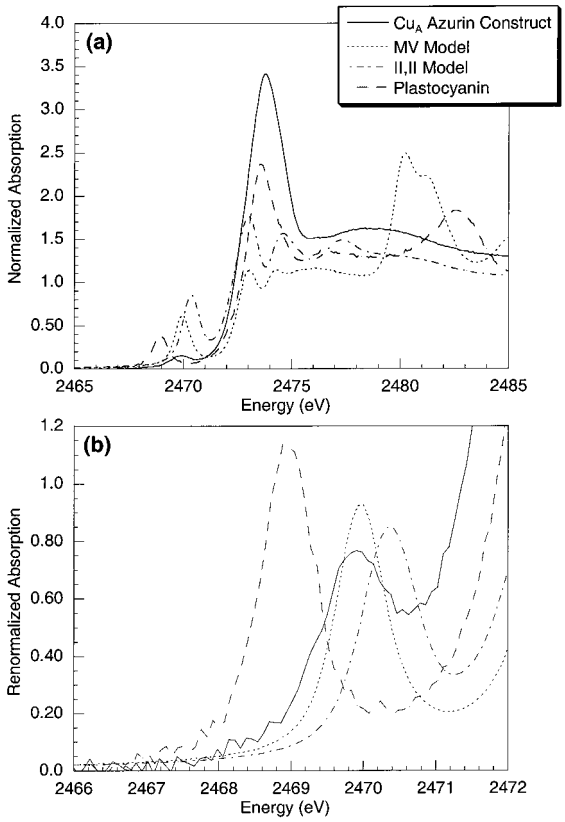


**Figure 2.** Comparison of (a) the normalized S K-edge spectra of the $Cu_A$ azurin construct, MV model, (II,II) model, and plastocyanin. (b) The renormalized pre-edge data (expanded scale) of the samples shown in (a).

**Table 1.** S K-Edge XAS Data Fit Results

| compound | pre-edge energy (eV)[a] | renormalized pre-edge intensity[b] | %S[b] covalency | total HOMO S covalency[b,c] |
|---|---|---|---|---|
| $Cu_A$ | 2469.9 | 0.65 | 23 | 46 ± 2.0 |
| MV model | 2470.0 | 0.73 | 27 | 54 ± 2.5 |
| (II,II) model | 2470.4 | 0.69 | 26 | 26 ± 1.0 |
| plastocyanin[d] | 2469.0 | 1.02 | 38 | 38 |

[a] Energies reported are within an error of ±0.1 eV. [b] The %S covalency has been renormalized to account for the different number of sulfurs which contribute to the pre-edge and edge features. The total HOMO S covalency takes the number of sulfurs and the number of d-holes into account. [c] Error reported is the standard deviation of all good fits; an additional 3% error is introduced by the normalization procedure. [d] Reference 14.

d-holes, these values are 23% S covalency for $Cu_A$, 27% for the MV model, and 26% for the homovalent model, Table 1). This is particularly important in our understanding of $Cu_A$ and the MV model because similar sulfur covalencies indicate that the S superexchange contribution to electronic coupling between the Cu atoms ($2H_{Cu-Cu}$) is approximately equal for both mixed-valent $Cu_2S_2$ centers. However, based on previous absorption and MCD studies,[25] the class III mixed-valence $\psi \rightarrow \psi^*$ transition (which is equal to $2H_{Cu-Cu}$) increases from ~5600 $cm^{-1}$ in the mixed-valence model to ~13 400 $cm^{-1}$ in $Cu_A$.

(55) There are 10 sulfurs (six Met and four Cys) in the $Cu_A$ azurin construct, which all contribute to the edge jump, while only two (the Cys thiolates) contribute to the pre-edge. In plastocyanin, three sulfurs contribute to the edge jump (two Met and one Cys), while only the Cys thiolate contributes to the pre-edge. In the MV model complex, three sulfurs (two thiolates and a triflate anion) contribute to the edge jump, while two thiolates contribute to the pre-edge. In the homovalent model complex, both sulfurs contribute to the edge jump and pre-edge.

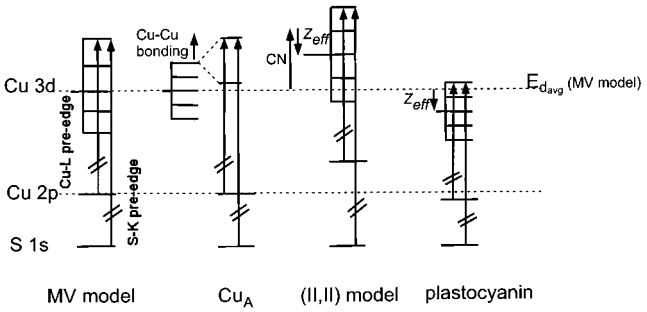


**Figure 3.** Comparison of the contributions to the Cu L-pre-edge and S K-pre-edge transition energies. $E_{d\ avg}$ is the average energy of the d manifold.

This implies that the additional (~7800 $cm^{-1}$) contribution to $H_{Cu-Cu}$ in $Cu_A$ is due to a direct Cu−Cu bonding interaction, which is not present in the MV model in which the relatively long Cu−Cu distance (2.9 Å) precludes metal−metal bonding.

As shown above, the S covalencies for $Cu_A$, the MV model, and the homovalent (II,II) model are 23%, 27%, and 26% S 3p, respectively. However, since the pre-edge feature is normalized to one sulfur and there are two sulfurs contributing to the single d-hole of the delocalized dimers, the covalencies for $Cu_A$ and the MV model must be doubled, giving values 46% and 54%, respectively. Thus, $Cu_A$ has a slightly larger S(Cys)−Cu anisotropic covalency than plastocyanin, but it is distributed over two S(Cys) ligands.

**(ii) Pre-edge Energies.** As indicated in Table 1, within the resolution of the data, the pre-edge transitions (S 1s → HOMO) of $Cu_A$ and the MV model are at the same energy (2469.9 and 2470.0 eV for $Cu_A$ and MV model, respectively), while the homovalent model pre-edge feature is at a higher energy, 2470.4 eV.

On the basis of the similar S covalencies of $Cu_A$ and the MV model, the energies of the S 1s orbitals, which depend on charge donation, are assumed to be the same.[56] Since the pre-edge transitions are at the same energy, the HOMOs must also be at the same or very similar energies (Figure 3). There are three main factors that contribute to the energy of the HOMO: the ligand-field-induced splitting of the d-manifold, the effective nuclear charge ($Z_{eff}$) on the metal center, and the potential contribution from metal−metal bonding. Previous spectroscopic studies combined with calculations have indicated that the ligand field of $Cu_A$ is ~0.4 eV weaker than that in the MV model.[25] In addition, $Z_{eff}$ is expected to be, if anything, slightly higher in $Cu_A$ due to the decrease in coordination number (from 4-coordinate in the MV model to ~3.5-coordinate in $Cu_A$). These would both decrease the energy of the HOMO.[57] Considering the combined effects of decreased ligand field splitting and higher $Z_{eff}$ in $Cu_A$, the S 1s → HOMO pre-edge transition of $Cu_A$ would be expected to be at least 0.4 eV to lower energy than this transition in the MV model. The equivalent pre-edge energies of the protein and the model indicate that a metal−metal bonding contribution raises the energy of the HOMO in $Cu_A$ by at least 0.4 eV.

The increase in the pre-edge energy of the homovalent model relative to that of the MV model can be assigned in a similar manner (Figure 3). The similar S covalency and essentially identical rising edge inflection points indicate that the S 1s cores of the MV model and the homovalent model are at the same

(56) Glaser, T.; Hedman, B.; Hodgson, K. O.; Solomon, E. I. *Acc. Chem. Res.* **2000,** *33,* 859−868.

(57) The change in $Z_{eff}$ on going from the MV model to $Cu_A$ is expected to be small since the effect of reducing the ligand−donor interaction will be less for Cu(1.5) than for Cu(II).

energy.[58] The 0.4 eV increase in energy on going from the MV model to the homovalent model thus reflects a shift in the energy of the half-occupied HOMO. From ref 25, the ligand field splitting of these two models is approximately equal and thus will not contribute to a shift in the half-occupied HOMO energy. The higher $Z_{eff}$ on the homovalent model (an increase by one-half of an oxidation state) will tend to decrease the energy of d-manifold, including the HOMO. However, this effect is countered by the increase in coordination number (from 4-coordinate in the MV model to 5-coordinate in the homovalent model). S K-edge studies on model complexes have shown that for a Cu(II) complex, addition of a ligand will increase the energy of the HOMO by ~0.6−1.0 eV.[59] The total effect of the increased $Z_{eff}$ and coordination number leads to a 0.4 eV increase in HOMO energy, and from this it can be estimated that an increase by one-half of an oxidation state at copper alone results in a decrease in the energy of the HOMO by 0.2−0.6 eV. This is consistent with pre-edge shifts observed at metal K-edges.[60−62]

Comparison of the relative pre-edge energies of $Cu_A$ and plastocyanin is of particular interest. As shown in Figure 2 and Table 1, the pre-edge energy of $Cu_A$ is 0.9 eV higher than that of plastocyanin. The similar S covalencies of $Cu_A$ and plastocyanin suggest that the S 1s cores should be at similar energy and thus imply that the 0.9 eV difference is due primarily to a shift in the HOMO. The ligand field strengths are essentially identical for $Cu_A$[25] and plastocyanin[63,64] and thus will not contribute to a shift in the HOMO. However, the lower $Z_{eff}$ of $Cu_A$ relative to that of plastocyanin will shift the d-manifold to lower binding energy (by ~0.2−0.6 eV, vide supra). In addition, the metal−metal bonding contribution in $Cu_A$ will further raise the d-manifold energy. The overall increase in energy of the HOMO of 0.9 eV thus implies a 0.3−0.7 eV contribution from metal−metal bonding, again within the range of previous estimates.[25]

**B. Cu L-Edges. (i) Intensities.** A comparison of the normalized Cu L-edge spectra for the $Cu_A$ azurin construct, the MV model, the homovalent (II,II) model, and plastocyanin is shown in Figure 4a. All four samples exhibit an $L_3$ transition maximum at ~931 eV and an $L_2$ transition maximum at ~951 eV. The intensity of the pre-edge features in the homovalent (II,II) model is similar to that in plastocyanin, while the intensities of the pre-edge features for both the MV model and $Cu_A$ azurin construct are decreased by a factor of ~2. This decrease on going from the homovalent (II,II) model to the MV model is consistent with reduction by one electron. Figure 4b shows the data renormalized to account for the number of d-holes.

To quantify the Cu d character in the HOMO, the integrated intensity of the $L_3 + L_2$ peaks is referenced to that of $D_{4h}$ $[CuCl_4]^{2-}$, for which the integrated area corresponds to 61% Cu d character.[15] On the basis of comparison to $D_{4h}$ $[CuCl_4]^{2-}$, previous studies indicated 41% Cu d character in the HOMO of plastocyanin[15] (Table 2). Similarly, the integrated intensity (Table 2) gives 43% d character per Cu for the homovalent (II,II) model. For the MV model and $Cu_A$ azurin, integration yields 19% and 22% d character per Cu, or total HOMO contributions of 38% and 44%, respectively. The L-edge results thus indicate very similar d character for plastocyanin and $Cu_A$, but in $Cu_A$ the d character is distributed over two metal centers.

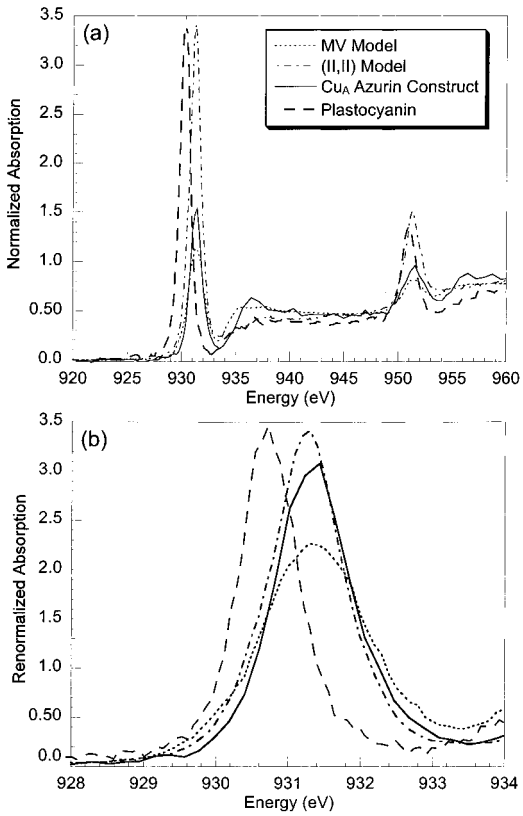


**Figure 4.** (a) Comparison of the normalized Cu L-edge spectra of the $Cu_A$ azurin construct, MV model, (II,II) model, and plastocyanin. (b) The renormalized $L_3$ data (expanded scale) of the samples shown in (a).

**Table 2.** Cu L-Edge XAS Data Fit Results

| compound | peak positions (eV)[a] $L_3$ | peak positions (eV)[a] $L_2$ | $L_3 + L_2$ peak intensity | covalency per Cu (%) | total HOMO Cu covalency[b] |
|---|---|---|---|---|---|
| $Cu_A$ | 931.4 | 951.5 | 2.99 | 22 | 44 ± 1.0 |
| MV model | 931.3 | 951.4 | 2.60 | 19 | 38 ± 0.4 |
| (II,II) model | 931.2 | 951.3 | 5.95 | 43 | 43 ± 1.7 |
| plastocyanin[c] | 930.7 | *d* | | 41 | 41 |
| $D_{4h}$ $CuCl_4^{2-}$ | 931.0 | 951.0 | 8.52 | 61 | 61 ± 2.0 |

[a] Energies reported are within an error of ±0.1 eV. [b] Error reported is the standard deviation of all good fits; an additional 4% error is introduced by the normalization procedure. [c] Reference 15. [d] $L_2$ edge energy and peak intensities were not reported in ref 15.

**(ii) $L_3$ and $L_2$ Pre-edge Energies.** The relative $L_3$- and $L_2$-pre-edge peaks' energies are given in Table 2. The $L_3$- and $L_2$-pre-edge features correspond, respectively, to transitions from $2p_{3/2}$ and $2p_{1/2}$ hole final states to the HOMO. In understanding the Cu L-edge energies, there are three main factors to consider: the effective nuclear charge ($Z_{eff}$), the ligand field-induced splitting of the d-manifold, and any potential contribution from metal−metal bonding. A change in $Z_{eff}$ will affect both the Cu 2p and 3d orbital energies. Calculations have

(58) Note, in our analysis of the pre-edge energies of $Cu_A$ and the MV model, the S K-edge rising edge inflection point could not be used as a measure of the S 1s core position due to the different nature of the thiolates.

(59) George, S. D.; Hedman, B.; Hodgson, K. O.; Solomon, E. I., unpublished results.

(60) Westre, T. E.; Kennepohl, P.; DeWitt, J. G.; Hedman, B.; Hodgson, K. O.; Solomon, E. I. *J. Am. Chem. Soc.* **1997**, *119*, 6297−6314.

(61) DuBois, J. L.; Mukherjee, P.; Solomon, E. I.; Stack, T. D. P.; Hodgson, K. O. *J. Am. Chem. Soc.* **2000**, *122*, 5775−5787.

(62) Brant, P.; Squire, K. R.; Canich, J. M.; Stevens, P. A.; DeVries, B.; Matsunaga, P.; Sansone, M.; Christopher, J.; Via, G. H. Stibrany, R.; Solomon, E. I., manuscript in preparation.

(63) Gewirth, A. A.; Solomon, E. I. *J. Am. Chem. Soc.* **1988**, *110*, 3811−3819.

(64) LaCroix, L. B.; Shadle, S. E.; Wang, Y. N.; Averill, B. A.; Hedman, B.; Hodgson, K. O.; Solomon, E. I. *J. Am. Chem. Soc.* **1996**, *118*, 7755−7768.

**Table 3.** Orbital Spin Populations (×100) of the Ground State Wave Functions[a] in the Means of Mulliken and Weinhold Population Analyses

| | | | ROB3LYP Mulliken | | | | UB3LYP Mulliken | | | | UB3LYP Weinhold[c] | | | |
|---|---|---|---|---|---|---|---|---|---|---|---|---|---|---|
| symbol[b] | PDB ID | atom no.[b] | Σ | d | s | p | Σ | d | s | p | Σ | d | s | p |
| $Cu^S$ | Cu632 | 1 | 23 | 23[d] | 0 | 0 | 20 | 22[f] | −1 | −1 | 21 | 23 | −1 | −1 |
| $Cu^O$ | Cu631 | 2 | 25 | 25[e] | 0 | 0 | 22 | 25[g] | −1 | −2 | 23 | 25 | −1 | −1 |
| $S^S$ | S$\gamma$CYS612 | 39 | 18 | 0 | 0 | 18 | 22 | 0 | 1 | 21 | 20 | 0 | 0 | 20 |
| | C$\beta$CYS612 | 38 | 0 | 0 | 0 | 0 | −1 | 0 | 0 | −1 | −1 | 0 | 0 | −1 |
| | H$\gamma$CYS612 | 41 + 42 | 1 | | 1 | | 1 | | 1 | | 1 | | 1 | |
| $S^O$ | S$\gamma$CYS616 | 22 | 26 | 0 | 0 | 26 | 30 | 0 | 1 | 29 | 30 | 0 | 1 | 29 |
| | C$\beta$CYS616 | 21 | 0 | 0 | 0 | 0 | −1 | 0 | 0 | −1 | −1 | 0 | 0 | −1 |
| | H$\gamma$CYS616 | 24 + 25 | 1 | | 1 | | 1 | | 1 | | 2 | | 2 | |
| $N^S$ | N$\delta$HIS546 | 44 | 3 | 0 | 1 | 2 | 3 | 0 | 1 | 2 | 2 | 0 | 0 | 2 |
| | C$\epsilon$HIS546 | 46 | 0 | 0 | 0 | 0 | 0 | 0 | 0 | 0 | −1 | 0 | −1 | 0 |
| $N^O$ | N$\delta$HIS620 | 13 | 2 | 0 | 1 | 1 | 3 | 0 | 1 | 2 | 1 | 0 | 0 | 1 |
| | C$\epsilon$HIS620 | 14 | 0 | 0 | 0 | 0 | 0 | 0 | 0 | 0 | 1 | 0 | 0 | 1 |
| | H(C)$\beta$HIS620 | 17 | 0 | | 0 | | 0 | | 0 | | 1 | | 1 | |
| O | O_GLU614 | 34 | 0 | 0 | 0 | 0 | 0 | 0 | 0 | 0 | 0 | 0 | 0 | 0 |
| S | S$\delta$MET623 | 4 | 0 | 0 | 0 | 0 | 0 | 0 | 0 | 0 | 0 | 0 | 0 | 0 |
| atoms not listed in this table | | | 1 | | | | 0 | | | | 1 | | | |

[a] ROB3LYP: $E_{total} = -5336.01845584$ au, $\langle S^2 \rangle = 0.7500$. UB3LYP: $E_{total} = -5336.02005083$ au, $\langle S^2 \rangle = 0.7577$. [b] Symbols and atom numbers are as given in Chart 1. Superscript S and O indicate the axial ligand, S = S$\delta$MET623, O = O_GLU614. [c] Cu: core 1s−3p; valence 3d,4s; Rydberg 4p and higher. [d] $z^2$ 0 $xz$ 0 $yz$ 0 $x^2 - y^2$ 20 $xy$ 3. [e] $z^2$ 1 $xz$ 0 $yz$ 0 $x^2 - y^2$ 24 $xy$ 1. [f] $z^2$ 0 $xz$ 0 $yz$ 0 $x^2 - y^2$ 20 $xy$ 2. [g] $z^2$ 0 $xz$ 0 $yz$ 0 $x^2 - y^2$ 25 $xy$ 0.

estimated that a 1.0 eV shift of the 2p orbital will result in a corresponding 0.86 eV shift in the 3d orbital.[65] Hence, only large changes in $Z_{eff}$ (which result in a greater than 1 eV shift in the 2p orbital) will result in a change in the 2p → 3d transition energy that is experimentally observable (i.e., a change that is greater than the 0.1 eV resolution of the experiment). In contrast, for S K-edges where only the 3d manifold is affected by $Z_{eff}$, there is no cancellation, and the effect is large. Alternatively, the contributions from ligand field and metal−metal bonding to the Cu L-edge will affect only the HOMO and thus are more readily probed by this technique.

From Figure 4 and Table 2, the $L_3$- and $L_2$-pre-edge peaks for $Cu_A$ azurin are at 931.4 and 951.5 eV, respectively, and are (within the error of the resolution) at the same energies as the $L_3$- and $L_2$-pre-edge peaks of the MV model. On the basis of analysis of the S−K pre-edge energies (vide supra), the HOMO has been determined to be at the same energy for $Cu_A$ and the MV model. Thus, the essentially identical L-edge energies indicate that the change in $Z_{eff}$ between the MV model and $Cu_A$ are not large enough to be experimentally observed by this method (Figure 4). Attention can then be turned to the similar HOMO energy. As in the case of the S K-edges energy analysis, this is attributed to two effects. The first is a decrease in the ligand field of $Cu_A$ relative to the MV model that results in a d-manifold shift to ∼0.4 eV lower energy. The second countering effect is due to an ∼0.4 eV contribution from metal−metal bonding which increases the energy of the HOMO. This is in agreement with the S K-edge results, which also showed an ∼0.4 eV contribution from metal−metal bonding. In addition, it is consistent with MCD and absorption data, which indicate an ∼7800 $cm^{-1}$ contribution to $2H_{Cu-Cu}$ or an effective increase of ∼3900 $cm^{-1}$ (∼0.5 eV) in the energy of the HOMO due to direct Cu−Cu interaction.[25]

The Cu L-pre-edge energies of the homovalent model relative to those of the MV model can be analyzed in an analogous manner. As shown in Table 2, the $L_3$- and $L_2$-pre-edge energies of the homovalent model are the same, within the resolution of the data, as those of the MV model (931.2 and 951.3 eV for the homovalent model, and 931.3 and 951.4 eV for the MV model). As described above, the essentially identical ligand fields of these two complexes indicate there should be no difference in the HOMO energies resulting from ligand field-induced splitting of the d-manifold. However, on the basis of the S K-edge analysis, it was estimated that the HOMO energy increased by 0.4 eV (due to a net decrease in $Z_{eff}$) on going from the MV model to the homovalent model. However, this change in $Z_{eff}$ will also affect the Cu 2p orbital, and, as described above, this will mostly cancel, leading to a less than 0.1 eV expected change in energy, which is consistent with these results.

A comparison of the Cu L-pre-edge energies of $Cu_A$ and plastocyanin (Figure 4, Table 2) shows that the $L_3$ and $L_2$ peaks of $Cu_A$ are ∼0.7 eV higher in energy. The similarity in the ligand fields of these two proteins indicates that this contribution should not change the energy. The contribution from a change in $Z_{eff}$ is again expected to be small and would, if anything, shift the $Cu_A$ pre-edge energies down (formal charge of +1.5 vs +2). Therefore, the increase in energy of ∼0.7 eV is a direct reflection of a metal−metal bonding contribution to the energy of the HOMO.

**C. Electronic Structure Calculations.** A representative analysis of the DFT calculation for the $Cu_A$ active site is shown in Table 3. In the text, only values obtained by the Mulliken population analysis are discussed, since the Weinhold population analysis gives equivalent results.

In the spin-restricted calculations, the total spin density over both Cu atoms is 48%, which breaks down to 44% $d_{x^2-y^2}$, 4% $d_{xy}$, and less than 1% 4s + 4p contributions. The spin density for both sulfur atoms (44%) has p character without any significant s or d contribution. The imidazole N and Cys $\beta$-methylene H atoms contribute 5% and 2%, respectively. The different nature of the α and $\beta$ orbitals in the spin-unrestricted treatment is apparent from the population analysis. The spin polarization introduces a small negative spin density, which is mainly located on the Cu s + p and Cys $\beta$-methylene C atoms. This is the result of the different mixing of the basis functions (i.e., atomic orbitals) in the occupied $\beta$-MOs relative to the α-set.

The total atomic spin densities are similar to those obtained by spin-restricted calculations, yet some differences should be noted. Due to spin polarization, the net positive spin density

(65) Kennepohl, P.; Solomon, E. I., unpublished results.

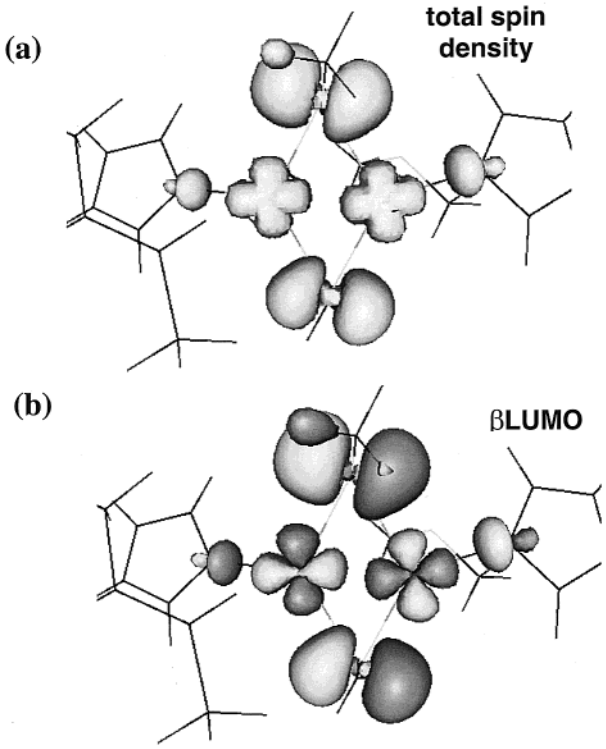


**Figure 5.** (a) Total spin density and (b) spin-down counterpart of the singly occupied HOMO ($\beta$LUMO) molecular orbitals of the $Cu_A$ model system (contour values = 0.001 and ±0.035 au).

on the $Cu_2$ unit is decreased, while the spin density on the Cys $S_2$ unit is increased (−5% and +7%, respectively).

The pure $\beta$LUMO properties were determined using the modified population analysis (see Experimental Section). The calculated total contribution of both the $Cu_2$ and the Cys $S_2$ moieties to the $\beta$LUMO is 46%, which has less than 1% Cu s + p and 1% S s + d contributions. These values are quite similar to the total spin density values ($Cu_2$ difference −3%, Cys $S_2$ +5%), which supports our assumption that the $\beta$LUMO reflects the total spin density. The agreement for the His N atoms and Cys $\beta$-methylene H atoms is also good (total spin density, $N_2$ is 6%, $H_2$ is 2%; $\beta$LUMO, $N_2$ is 4%, $H_2$ is 1%). Beyond the numerical results, the similarity is well demonstrated by comparison of the contour plots of the total spin density and the $\beta$LUMO (Figure 5). These contours also present the major components of the ground-state wave function and are in excellent agreement with the Cu L- and S K-edge experimental results. The ground-state wave function is discussed in detail in the next section.

## Discussion

**A. Nature of the Ground-State Wave Function.** By combining the experimental and theoretical results, an estimate of the total ground-state wave function can be obtained. The $\beta$LUMO (as defined in eq 1) is considered in detail, since this is the redox-active orbital of the $Cu_A$ active site and the orbital that is probed by the metal L- and ligand K-edge spectroscopies.[66]

As shown in Figure 5, the ground-state wave function consists of four major contributions: the Cu, bridging Cys S, imidazole $\delta$-N, and Cys $\beta$-methylene H atoms. This is consistent with the Cu L-edge and S K-edge experiments, which show 44% Cu d and 46% S p contributions, respectively. These values correspond to the $\beta$LUMO covalencies determined via theory. Further, from $^{14,15}$N-ENDOR[27,67] and $^1$H-ENDOR[27] studies, the total contributions of the imidazole N and $\beta$-methylene H atoms are found to be ~6%[68] and ~3%. These values can be directly correlated with the total atomic spin density.

On the basis of the calculations in Table 3, the $\beta$LUMO reflects the total spin density, as it reflects the α spin not compensated by a $\beta$ electron in a valence orbital. The experimentally measured values (Cu d + S p + N total + H total) comprise ~99 ± 7%.

Additional small contributions may be attributed to Cu s + p, S s + d components and to the remaining atoms. Evidence for a small amount of Cu 4p/3d mixing is observed in the Cu K-edge spectrum of $Cu_A$, which shows a very weak pre-edge feature (Figure S1, Supporting Information). Quantifying the pre-edge intensity of $Cu_A$ relative to $D_{4h}$ $[CuCl_4]^{2-}$ indicates ~1% 4p mixing into the ground state of $Cu_A$. A small contribution from the S 3s orbital is also possible through hybridization and is observed computationally (~1%). Minor contributions from the Cys $\beta$-methylene C atoms and the noncoordinated imidazole ring atoms are also anticipated.

**B. Comparison to Plastocyanin.** To allow for comparison to $Cu_A$, it is important to similarly define the ground-state wave function of plastocyanin. For plastocyanin, combined Cu L-edge (41% Cu d)[15] and S K-edge (38% S)[14] results account for 79% of the ground-state wave function. ENDOR studies on the classic blue copper sites in plastocyanin[69] and azurin[70] indicate that an additional ~9% character resides on the nitrogen atoms of the histidines,[71] thus accounting for ~88 ± 7% of the wave function. On the basis of calculations on plastocyanin, additional contribution are attributed to the $\beta$-methylene protons (~3%),[17] Cu 4s/p (~4%),[50] S s/d (~2%),[50] and the remaining atoms.

From Tables 1 and 2, plastocyanin and $Cu_A$ have similar total sulfur contributions to the HOMO (38% S for plastocyanin and 46% S for $Cu_A$), as well as similar Cu d character (41% Cu for plastocyanin and 44% Cu for $Cu_A$). The important difference is that in $Cu_A$, the total sulfur covalency is delocalized over two sulfurs and the total Cu d character is delocalized over two coppers. It is this delocalization which has important significance for the ET function of $Cu_A$.

**C. Functional Significance. (i) Reorganization Energy.** The L-edge studies show that a similar total charge is delocalized over the two Cu ions in $Cu_A$ relative to blue copper. It has been suggested that this delocalization should lower both the inner- and outer-sphere reorganization energy ($\lambda$) of $Cu_A$.[25] By using an excited-state distortion analysis of the resonance Raman enhancement profile for $Cu_A$ and plastocyanin, estimates of the inner-sphere reorganization energy have been obtained. This gives ~2000 $cm^{-1}$ for $Cu_A$[25] and ~3900 $cm^{-1}$ for plastocyanin.[72] Experimental values have also been obtained for the total

(66) It should be noted that electronic relaxation has a negligible effect on the valence region of the wave function in the S 1s → $\Psi^*$ transition, since no shake-up transitions are observed experimentally or established from theoretical calculations. Relaxation would charge-compensate for the hole produced on the ligand via a metal-to-ligand charge-transfer process, which is not accessible with donor ligands.

(67) Gurbiel, R. J.; Fann, Y. C.; Surerus, K. K.; Werst, M. M.; Musser, S. M.; Doan, P. E.; Chan, S. I.; Fee, J. A.; Hoffman, B. M. *J. Am. Chem. Soc.* **1993**, *115*, 10888−10894.

(68) This value is based on the average total spin density from ENDOR studies on C*c*O and nitrous oxide reductase.

(69) Werst, M. M.; Davoust, C. E.; Hoffman, B. M. *J. Am. Chem. Soc.* **1991**, *113*, 1533−1538.

(70) Coremans, J. W. A.; Poluektov, O. G.; Groenen, E. J. J.; Canters, G. W.; Nar, H.; Messerschmidt, A. *J. Am. Chem. Soc.* **1996**, *118*, 12141−12153.

(71) This value is based on the average spin density from ENDOR studies on plastocyanin and azurin.

(72) Fraga, E.; Webb, M. A.; Loppnow, G. R. *J. Phys. Chem.* **1996**, *100*, 3278−3287.

reorganization energy in $Cu_A$ and blue copper proteins. For the blue copper protein azurin, the total reorganization ($\lambda_{blueCu}$) energy is 0.8 eV.[73−75] For $Cu_A$, the experimentally determined value is 0.3−0.4 eV ($\lambda_{CuA}$),[76,77] or at least a factor of 2 lower than blue copper. Comparing these numbers to the estimated inner-sphere reorganization energies (and using a value of 0.4 eV for $\lambda_{CuA}$), values of 0.15 and 0.32 eV are obtained for the outer-sphere reorganization energies of $Cu_A$ and blue copper, respectively. This indicates that both the inner- and outer-sphere reorganization energies are lowered by a factor of ∼2 in $Cu_A$.

The functional significance of this change in reorganization energy can be estimated from its effect on the $Cu_A$ → heme *a* electron-transfer rate (i.e., substitution of $\lambda_{blueCu}$ for $\lambda_{CuA}$, where $\lambda_{total} = (\lambda_{CuA} + \lambda_{heme\ a})/2$ and $\lambda_{heme\ a} = 0.4$ eV[78]). This was done using the isotropic model for electron transfer:[79]

$$k_{ET} = 10^{13} \exp(-\beta d) \exp[-(\Delta G^\circ + \lambda)^2/4\lambda kT] \qquad (2)$$

where the decay parameter, $\beta$, was assumed to be 1.0 Å$^{-1}$ and *d*, which represents the donor−acceptor distance (minus 3 Å to account for van der Waals contact), is 16.5 Å.[18] For $Cu_A$ → heme *a* ET the driving force, $\Delta G^\circ$, is 0.05 eV.[13] This results in predicted electron-transfer rates of $4.9 \times 10^4$ s$^{-1}$ for $Cu_A$ → heme *a* and $7.2 \times 10^3$ s$^{-1}$ for the hypothetical blue copper → heme *a* pathway, demonstrating that the decreased total reorganization energy in $Cu_A$ can provide a factor of ∼7 enhancement in electron transfer to the heme *a* site.

**(ii) Pathways.** The nature of the ground-state wave function of $Cu_A$ has important implications for both intramolecular ET from $Cu_A$ to heme *a* and intermolecular ET from the heme *c* of cytochrome *c* into $Cu_A$. To test possible ET pathways, we applied the Pathways program developed by Beratan and Onuchic[80−87] to the 2.3 Å crystal structure of bovine C*c*O.[88] This program is based on the idea that the electronic coupling matrix element ($H_{AB}$) of an ET pathway can be described as a product of decay factors of the individual covalent ($\epsilon_C$), hydrogen bonds (H bonds, $\epsilon_H$), and through-space jumps ($\epsilon_S$), such that

$$H_{AB} = H_{AB}{}^0 \Pi\epsilon_C \Pi\epsilon_H \Pi\epsilon_S \qquad (3)$$

The values used for these decay parameters are as follows:

$$\epsilon_C = 0.6 \qquad (4)$$

$$\epsilon_S = \epsilon_C \exp[-1.7(R - 1.4)] \qquad (5)$$

$$\epsilon_H = \epsilon_C, \quad R \le 1.8\ \text{Å} \qquad (6)$$

$$\epsilon_H = \epsilon_C \exp[-1.7(R - 1.8)], \quad R > 1.8\ \text{Å} \qquad (7)$$

The coupling decay across one covalent bond, $\epsilon_C$, is an empirically determined value. The decay across a space jump is considered exponential with distance, *R*. In eq 5, the 1.4 Å distance represents an average orbital center-to-center equilibrium distance. The criterion for what constitutes an H bond is less well defined. In eqs 6 and 7, *R* is the H atom to H bond, accepting heavy atom distance. This set of equations allows for exponential decay for H bonds longer than 1.8 Å. This value is based on H bond distances obtained from neutron diffraction studies[89] and is consistent with previous Pathways analyses.[79]

In addition to the decay coupling as described by the Pathways program, the coupling of the metal d orbitals in to and out of the hole superexchange pathway must also be considered.[16,17] The S K-edge data combined with the N ENDOR[27,67] data show that the redox-active orbital in Figure 5 is highly anisotropic, with the S bonds being the most covalent. In the McConnell superexchange mechanism, the effect of coupling in to and out of the bridge on $H_{AB}$ is incorporated into the prefactor, $H_{12}/\Delta E_{12}$, where $H_{12}$ is the metal−ligand resonance integral and $\Delta E_{12}$ is the ligand-to-metal charge-transfer energy.[90] $H_{12}/\Delta E_{12}$ is equal to the HOMO wave function coefficient, which is in turn equal to the square root of the covalency. Thus, for a given bridge and final state, $k_{ET}$ is proportional to the metal−ligand covalency, and for comparison of the rates derived by the Pathways program, $k_{ET}$ must be weighted by the appropriate ligand character in the redox-active $\beta$LUMO orbital.

**(a) Intramolecular ET, $Cu_A$ → Heme *a* Pathway.** Three primary pathways to the heme *a* in subunit I at a distance of ∼19.5 Å were considered in the Pathways analysis (as shown in Figure 6): one through the His204, a second through the Cys200, and a third through the Cys196. The pathway via His204 is the same as the ET pathway previously identified by Regan et al.[91] This pathway involves 14 covalent bonds and 2 H bonds (one short H bond at 1.87 Å and one longer H bond at 2.35 Å). The overall decay coupling for this pathway is $1.3 \times 10^{-4}$ (Table 4). This decay coupling gives $\beta = 1.08$ Å$^{-1}$, corresponding to a predicted ET rate of $1.3 \times 10^4$ s$^{-1}$, in good agreement with the experimental rate. The second pathway, via the Cys200, is very similar to that identified by Medvedev et al.[92] Involving a total of 17 covalent bonds, this pathway travels from Cys200 to Ile199, through a short 1.83 Å H bond to Arg439, then through a 1.92 Å space jump to the propionate

(73) Di Bilio, A. J.; Hill, M. G.; Bonander, N.; Karlsson, B. G.; Villahermosa, R. M.; Malmström, B. G.; Winkler, J. R.; Gray, H. B. *J. Am. Chem. Soc.* **1997**, *119*, 9921−9922.
(74) Skov, L. K.; Pascher, T.; Winkler, J. R.; Gray, H. B. *J. Am. Chem. Soc.* **1998**, *120*, 1102−1103.
(75) The value for the reorganization energy for azurin is based on extensive experimental studies on Ru-modified azurins. It should be noted, however, that a value of 1.2 eV has been determined for one Ru-modified plastocynin (Sigfridsson, K.; Ejdeback, M.; Sundahl, M.; Hansson, O. *Arch. Biochem. Biophys.* **1998**, *351*, 197−206). This value is higher than the 0.8 eV value used in the ET calculation that follows and would result in additional enhancement of the $Cu_A$ ET path relative to blue copper.
(76) Brezezinski, P. *Biochemistry* **1996**, *35*, 5611−5615.
(77) Farver, O.; Lu, Y.; Ang, M. C.; Pecht, I. *Proc. Natl. Acad. Sci. U.S.A.* **1999**, *96*, 899−902.
(78) Farver, O.; Einarsdóttir, O.; Pecht, I. *Eur. J. Biochem.* **2000**, *267*, 950−954.
(79) Gray, H. B.; Winkler, J. R. *Annu. Rev. Biochem.* **1996**, *65*, 537−561.
(80) Beratan, D. N.; Hopfield, J. J. *J. Am. Chem. Soc.* **1984**, *106*, 1584−1594.
(81) Beratan, D. N.; Onuchic, J. N.; Hopfield, J. J. *J. Chem. Phys.* **1987**, *86*, 4488−4498.
(82) Beratan, D. N.; Onuchic, J. N.; Betts, J. N.; Bowler, B. E.; Gray, H. B. *J. Am. Chem. Soc.* **1990**, *112*, 7915−7921.
(83) Beratan, D. N.; Betts, J. N.; Onuchic, J. N. *Science* **1991**, *252*, 1285−1288.
(84) Beratan, D. N.; Betts, J. N.; Onuchic, J. N. *J. Phys. Chem.* **1992**, *96*, 2852−2855.
(85) Betts, J. N.; Beratan, D. N.; Onuchic, J. N. *J. Am. Chem. Soc.* **1992**, *114*, 4043−4046.
(86) Onuchic, J. N.; Beratan, D. N. *J. Chem. Phys.* **1990**, *92*, 722−733.
(87) Regan, J. J.; Onuchic, J. N. *Adv. Chem. Phys.* **1999**, *107*, 497−553.
(88) Yoshikawa, S.; Shinzawa-Itoh, K.; Nakashima, R.; Yaono, R.; Yamashita, E.; Inoue, N.; Yao, M.; Fei, M. J.; Libeu, C. P.; Mizushima, T.; Yamaguchi, H.; Tomizaki, T.; Tsukihara, T. *Science* **1998**, *280*, 1723−1729.
(89) Cotton, F. A.; Fair, C. K.; Lewis, G. E.; Mott, G. N.; Ross, F. K.; Schultz, A. J.; Williams, J. M. *J. Am. Chem. Soc.* **1984**, *106*, 5319−5323.
(90) Newton, M. D. *Chem. Rev.* **1991**, *91*, 767−792.
(91) Regan, J. J.; Ramirez, B. E.; Winkler, J. R.; Gray, H. B.; Malmström, B. G. *J. Bioenerg. Biomembr.* **1998**, *30*, 35−39.
(92) Medvedev, D. M.; Daizadeh, I.; Stuchebrukhov, A. A. *J. Am. Chem. Soc.* **2000**, *122*, 6571−6582.

**Table 4.** Comparison of Experimental Rates with Pathways Analysis Results

| pathway | distance (Å) | experimental rate ($s^{-1}$) | decay coupling | calculated $\beta$ ($Å^{-1}$) | calculated rate ($s^{-1}$) | corrected rate ($s^{-1}$)[a] |
|---|---|---|---|---|---|---|
| **$Cu_A$ → heme *a*** | 19.5 | $1 \times 10^4$ | | | | |
| His204 to heme *a* | | | $1.3 \times 10^{-4}$ | 1.08 | $1.3 \times 10^4$ | $1.3 \times 10^4$ |
| Cys200 to heme *a* | | | $9.9 \times 10^{-6}$ | 1.39 | $8.0 \times 10^1$ | $1.8 \times 10^3$ |
| Cys196 to heme *a* | | | $1.7 \times 10^{-6}$ | 1.56 | 2.0 | $4.8 \times 10^1$ |
| **Heme *c* → $Cu_A$** | 17.8 | $6 \times 10^4$ | | | | |
| 3.3 Å Trp CZ3 to heme CBC jump | | | $7.1 \times 10^{-6}$ | 1.60 | 3.8 | 90 |
| 1.4 Å Trp CZ3 to heme CBC jump | | | $3.0 \times 10^{-4}$ | 1.17 | $2.2 \times 10^3$ | $5.1 \times 10^4$ |

[a] The corrected rate accounts for the greater anisotropic covalency of the Cu−S(Cys) bonds relative to the Cu−N(His) bonds.

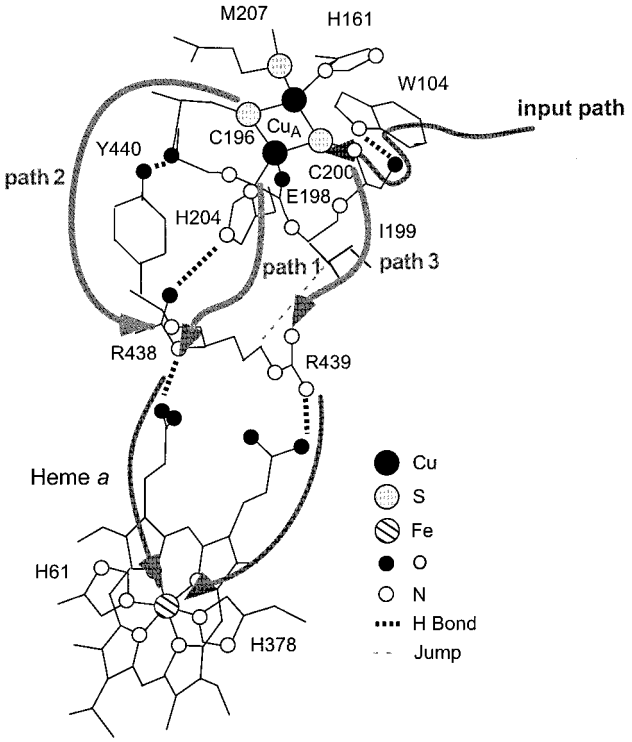


**Figure 6.** Proposed ET pathways in bovine heart C*c*O based on Pathways analysis. The Cys200 and His204 $Cu_A$-to-heme *a* pathways are potentially competitive in rate, while the Cys 196 pathway is significantly slower. The heme *c*-to-$Cu_A$ pathway via W104 is, however, expected to dominate due to the covalency of the $Cu_A$−S(Cys) bond.

chain and into the heme. The decay coupling for the Cys200 pathway is $9.9 \times 10^{-6}$, corresponding to a predicted rate of $8.0 \times 10^1$ $s^{-1}$. However, the greater Cu−S(Cys) covalency (23% per S) relative to the Cu−N(His) covalency (∼1−5%)[27,67] allows for enhancement of this rate by a factor of ∼5−23, increasing the rate to up to $1.8 \times 10^3$ $s^{-1}$. An additional enhancement factor for this pathway may derive from the more efficient coupling of the Cys S$\gamma$ orbitals with the Cys $\beta$-methylene protons, as compared to less efficient spin delocalization onto the His rings.[17] Taken together, these factors could make the Cys200 pathway competitive with the His204 pathway.[93] The pathway through Cys196[25] was also analyzed using the Pathways program. This path involves 24 covalent bonds and 2 H bonds and has a decay coupling of $1.7 \times 10^{-6}$. This gives a predicted rate of 2 $s^{-1}$. Accounting for anisotropic covalency, the rate is 48 $s^{-1}$, or still a factor of ∼270 slower than the His204 and Cys196 pathways, indicating that this pathway is not a major contribution in the $Cu_A$ to heme *a* ET path.

Pathways analysis of the $Cu_A$-to-heme *a* ET clearly indicates a favorable pathway via His204. Although paths through the Cys196 are less efficient, a third path through the Cys200 can be competitive with the His204 path when anisotropic covalency is taken into account. This leads to the possibility of multiple pathways[87] contributing to ET from $Cu_A$ to heme *a*, which could potentially further enhance the rate through interference effects. A quantitative assessment of this issue is beyond the scope of this analysis.

**(b) Intermolecular ET, heme *c* → $Cu_A$.** The ET path between cytochrome *c* and $Cu_A$ also deserves detailed consideration. Similar to the $Cu_A$-to-heme *a* ET pathway, the heme *c*-to-$Cu_A$ pathway has a rapid rate of ET (∼$6 \times 10^4$ $s^{-1}$),[94] a rather long distance, ∼18 Å, between the heme iron and $Cu_A$ (as predicted by modeling the docking of horse cytochrome *c* and bovine C*c*O),[95] and a very low driving force ($\Delta G° = -0.03$ eV).[96] In addition, the reorganization energy of heme *c* ($\lambda_{\text{heme } c} = 1.2$ eV)[97−99] is much greater than that of heme *a* ($\lambda_{\text{heme } a} = 0.4$ eV).[78] These factors require very efficient coupling of these sites and, hence, efficient pathways.

The Pathways program was used to evaluate the input pathway from the surface of C*c*O into $Cu_A$. Since in contrast to blue copper centers, the $Cu_A$ center in C*c*O has no surface-accessible ligating residues, protein-based ET pathways into $Cu_A$ are functionally relevant. Mutagenesis experiments have shown that Trp104-II is a key residue in the ET pathway from the cytochrome *c* docking site to $Cu_A$.[100] The indole ring of this Trp is on the cytosol-exposed surface. The best pathway from the indole-exposed ring into the $Cu_A$ proceeds through this residue, across an H bond, and then through the $Cu_A$-ligating Cys200, into the $Cu_A$ core. This path involves six covalent bonds and has a decay coupling of $3.9 \times 10^{-3}$. To obtain an estimate of the total ET rate, the pathway from the heme *c* to the indole-exposed ring was estimated by using values from the predicted

(93) It should be noted that the calculated rate and decay couplings are based on a through-space decay parameter of $\epsilon_S = \epsilon_C \exp[-1.7(R - 1.4)]$, where the $r_0$ of 1.4 Å corresponds to the orbital center-to-center equilibrium distance. Although this is a reasonable approximation for through-space jumps between C, N, and O atoms, for a jump that occurs between H atoms (as for the Cys200 path) a smaller value of $r_0$ may be more appropriate. Adjusting $r_0$ to 0.6 (the atomic radius of two H atoms) results in a smaller decay coupling ($2.5 \times 10^{-6}$ for $r_0 = 0.6$) and a significant decrease in the predicted rate (5 $s^{-1}$).

(94) Geren, L. M.; Beasley, J. R.; Fine, B. R.; Saunders, A. J.; Hibdon, S.; Pielak, G. J.; Durham, B.; Millett, F. *J. Biol. Chem.* **1995**, *270*, 2466−2472.

(95) Roberts, V. A.; Pique, M. E. *J. Biol. Chem.* **1999**, *274*, 38051−38060.

(96) Pan, L. P.; Hibdon, S.; Liu, R.-Q.; Durham, B.; Millett, F. *Biochemistry* **1993**, *32*, 8492−8498.

(97) Wright, J. L.; Wang, K.; Geren, L.; Saunders, A. J.; Pielak, G. J.; Durham, B.; Millett, F. *ACS Adv. Chem. Ser.* **1998**, *254*, 99−110.

(98) Wuttke, D. S.; Bjerrum, M. J.; Winkler, J. R.; Gray, H. B. *Science* **1992**, *256*, 1007−1009.

(99) The value reported for $\lambda_{\text{heme } c}$ is based on the average of the values in refs 97 and 98, reduced by 0.1 eV to account for the decrease in reorganization energy due to complex formation (Scott, J. R.; McLean, M.; Sligar, S. G.; Durham, B.; Millett, F. *J. Am. Chem. Soc.* **1994**, *116*, 7356−7362).

(100) Witt, H.; Malatesta, F.; Nicoletti, N.; Brunori, M.; Ludwig, B. *J. Biol. Chem.* **1998**, *273*, 5132−5136.

docked complex of horse cytochrome *c* and bovine C*c*O, which shows that the closest approach of the indole ring to the heme is between the Trp104 CZ3 and the heme CBC, at a distance of 3.3 Å.[95] By treating this distance as a through-space jump between two carbon atoms and including the remaining five covalent bonds from the heme CBC to the iron, a decay coupling of $1.84 \times 10^{-3}$ is obtained. Combining this decay coupling with that determined for the indole ring-to-$Cu_A$ pathway gives a decay coupling of $7.12 \times 10^{-6}$ and $\beta = 1.60$ Å$^{-1}$, corresponding to a rather slow predicted rate of 3.8 s$^{-1}$. However, there is some variability in the distance of the through-space jump from the Trp 104 CZ3 and the heme CBC, particularly because this number was derived from modeling the docked static structures from two separate crystal structures. Allowing the Trp 104 CZ3 and heme CBC atoms to come within 1.4 Å of each other, so that the through-space jump is equivalent to a covalent bond, gives an upper limit for the rate of $2.2 \times 10^3$ s$^{-1}$, which is still significanlty slower than turnover ($6 \times 10^4$ s$^{-1}$). Importantly, including the anisotropic covalency of the Cu−S(Cys) bond brings this rate to $5.1 \times 10^4$ s$^{-1}$, which is consistent with the experimentally observed rate.

Aside from these quantitative pathways analyses, there are some general observations that support the role of anisotropic covalency in ET for $Cu_A$. In comparing the rates for $Cu_A \rightarrow$ heme *a* and heme *c* $\rightarrow Cu_A$ ET to those of other electron-transfer proteins with similar distances between redox centers,[101] the rates for C*c*O are particularly fast, while the driving force is low. Although there is clearly a contribution due to the low reorganization energy of the $Cu_A$ site (vide supra), the high anisotropic covalency of the Cu−S bond must also contribute to these rapid rates. This is particularly clear for the heme *c* $\rightarrow$ $Cu_A$ pathway, where inter-protein ET as well as the higher reorganization energy of the heme *c* (1.2 vs 0.4 eV for heme *a*) still results in a more rapid rate of ET than even $Cu_A \rightarrow$ heme *a* ($6 \times 10^4$ vs $1 \times 10^4$ s$^{-1}$ for $Cu_A \rightarrow$ heme *a*).

## Summary

The results of this study provide a detailed understanding of the ground-state electronic structure of $Cu_A$. In particular, the results of XAS S K-edge and Cu L-edge analyses of $Cu_A$ and two relevant thiolate-bridged model complexes provide additional experimental evidence for direct metal−metal bonding in $Cu_A$, which makes a major contribution to keeping the $Cu_A$ site delocalized in the low-symmetry protein environment. This delocalization lowers both the outer- and inner-sphere reorganization energy of $Cu_A$ and contributes to the rapid ET rates. The Cu L- and S K-edge results combined with previously reported ENDOR data[27,67] provide an experimental description of the ground-state wave function of $Cu_A$. We find that this description is supported by DFT calculations. The highly covalent Cu−S bonds in $Cu_A$ are shown to be an important factor in long-range ET, making a S(Cys) path competitive with a shorter N(His) pathway for intramolecular ET and being particularly important for the heme *c* $\rightarrow Cu_A$ intermolecular ET process.

**Acknowledgment.** We thank Dr. Tim Machonkin for helpful discussions on the pathways analysis, Marjorie Ang for preparation of the $Cu_A$ azurin mutant, John Cahoy and Jamie Schneider for synthesis of the model complexes, Dr. Jeff Regan at California Institute of Technology for providing us with the Pathways program, and Joe Barco and Prof. Tom Wandless at Stanford University for use of Insight II. This work was supported by NIH RR-01209 (K.O.H.), GM44380 (S.P.C.), GM47365 (W.B.T.); NSF CHE-9980549 (E.I.S.), CHE9502421 (Y.L.); and DOE OBER (S.P.C.). SSRL operations are funded by the Department of Energy, Office of Basic Energy Sciences. The SSRL Structural Molecular Biology program is supported by the National Institutes of Health, National Center for Research Resources, Biomedical Technology Program, and by the Department of Energy, Office of Biological and Environmental Research. M.M. thanks the Deutscher Akademischer Austausch Dienst (DAAD) for a postdoctoral fellowship.

**Supporting Information Available:** Cartesian coordinates of computational model in Chart 1, and normalized Cu K-edge spectrum of $Cu_A$ construct (PDF). This material is available free of charge via the Internet at http://pubs.acs.org.

JA004109I

(101) Page, C. C.; Moser, C. C.; Cehn, X.; Dutton, P. L. *Nature* **1999**, *402*, 47−52.